

Buildup dynamics of broadband Q-switched noise-like pulse

Ji Zhou^{1,2,3,*}, Yuhang Li^{1,2,3,*}, Qing Yang³, Yaoguang Ma^{3,‡} and Qiang Liu^{1,2}

¹Key Laboratory of Photonic Control Technology (Tsinghua University), Ministry of Education, Beijing 100084, China

²State Key Laboratory of Precision Measurement Technology and Instruments,
Department of Precision Instrument, Tsinghua University, Beijing 100084, China

³State Key Laboratory of Modern Optical Instrumentation,
College of Optical Science and Engineering, Zhejiang University, Hangzhou 310027, China

(Dated: December 15, 2021)

We investigate the buildup dynamics of broadband Q-switched noise-like pulse (QS-NLP) driven by slow gain dynamics in a microfiber-based passively mode-locked fiber laser. Based on shot-to-shot tracing of the transient optical spectra and qualitatively reproduced numerical simulation, we demonstrate that slow gain dynamics is deeply involved in the onset of such complex temporal and spectral instabilities of QS-NLP. The proposed gain dynamics model could contribute to deeper insight into such nonlinear phenomenon and transient dynamics simulation in ultrafast fiber laser.

I. INTRODUCTION

As a typical dissipative system, ultrafast fiber lasers are now increasingly regarded as an ideal platform to study complex dynamics ranging from stationary periodic mode-locking, quasi-periodic pulsating, exploding and chaos [1, 2]. Among these numerous nonlinear dynamics, noise-like pulse (NLP) is a typical illustration of partial mode locking which manifests as seemingly regular long pulses (0.1-1 ns, typically) train while actually resembling burst of sub-ps scale chaotic, noise-like inner fluctuations [3]. Earlier study demonstrated that NLP could circulate with a rather stable envelope at the fundamental roundtrip frequency of the laser cavity, in spite of inner chaotic evolution, while there are also increasing reports recently on Q-switched noise-like pulse (QS-NLP) where Q-switching instabilities are not negligible. In this case, the laser undergoes slow, quasi-periodic energy fluctuations while lasing in a pulsating radiation pattern [4–7]. When modulated by Q-switching instabilities, QS-NLP usually accumulates energy in a short time, with boosting peak power in the following specific roundtrips and subsequently decay to background noise [5, 8]. This temporal intensity dynamics gives rise to nonlinearity enhancement resulting in a broad averaged spectrum that could exceed gain spectral width, while on the other hand contribute to other nonlinear phenomena, e.g. rogue waves (RW)—featured with pronounced L-shaped statistics distribution of intensity [6, 7].

Although NLP has been investigated theoretically [9], and experimental optical time-stretching [5, 10, 11] or temporal mapping techniques [12] have been successfully in real-time tracing of the NLP dynamic evolution, previous research work focus mainly on the stationary NLP where gain was assumed to saturate instantaneously with the current energy of pulse [9, 13, 14]. This assumption does not agree with the nature of QS-NLP since

Q-switching instabilities related gain evolution usually involves distinct time-scales: pulse duration on a ns scale (<0.1 ns here), pulse train on a μ s scale and slow gain relaxation time on a ms scale (1–10 ms) [15, 16]. The non-instantaneous slow gain dynamics usually play a pivotal role in several nonlinear dynamics phenomena such as internal oscillations-inhibited stable soliton molecules [17], gain depletion guided long-range pulses attraction [18], gain dynamics-dominated interpulse repulsion [19], wavelength-dependent gain competition driven NLP [4], as well as QS-NLP here.

Incorporating a slow gain dynamic model, the present work reveals the underlying QS-NLP dynamics in a dispersion and nonlinearity managed fiber ring laser [7]. Combining real-time dispersive Fourier transform (DFT) measurement of transient spectra and numerical simulation, we experimentally and numerically obtain the temporal and spectral instabilities of QS-NLPs shown similarly to [5, 20] and demonstrate that the QS-NLP comes from roundtrip-to-roundtrip dynamic equilibrium between gain and loss. Our work provides deeper insight into the pulse dynamics of broadband QS-NLP as well as universal gain mechanism in fiber lasers. The proposed model can be used to study active fiber Kerr cavities [21, 22] and on-chip doped microresonator lasers [23].

II. EXPERIMENT

The experiment platform is NPE based fiber ring laser as sketched in Fig. 1. For the DFT measurement, the laser output is temporally stretched by a 1 km fiber with group-velocity dispersion of $\beta_2 = 20.3$ ps²/km at ~ 1030 nm and subsequently fed into 25 GHz detector (Newfocus Model1414) along with 33 GHz oscilloscope (Tektronix DPO73304DX). As a result, the implemented spectral resolution is ~ 0.9 nm, sufficient for measuring such broadband spectra with 20-dB-bandwidth greater than 100 nm [10].

Self-starting QS-NLP operation could be initiated by increasing pump power high than 400 mW with several certain intracavity polarization configuration. We

* These authors contributed equally.

† lyhTHU@gmail.com

‡ mayaoguang@zju.edu.cn

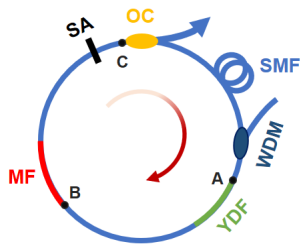


FIG. 1. Schematic configuration of the fiber ring laser in simulation, detailed information see [7]. MF: microfiber; SMF: Corning® HI1060; YDF: Yb-doped fiber; SA: saturable absorber; OC: output coupler. Intracavity position: A, 0/1.7 m; B, 0.6 m; C, 1.0 m; free space of 0.1 m ignored here.

deliberately pump the fiber laser at power of 600 mW to trigger QS-NLP with excess of gain. Fig. 2 shows the typical temporal intensity dynamics of QS-NLP in ms and μ s scale, where cavity-length-determined pulsing (duration of ~ 8.7 ns) is modulated by Q-switched envelope. At initial few roundtrips, due to stronger bleaching (i.e. positive feedback) effect of SA, the QS-NLP energy grows exponentially from slight relaxation oscillations [24]. The pulse energy grows continuously and thus saturates the gain rapidly. As a result, in the following remaining roundtrips loss has a greater impact than saturated gain and therefore results in to a slowly decaying trail of Q-switched envelope.

In the quasi-steady state where sampled averaged spectrum of spectrometer (Agilent 86142B) keeps seemingly fixed, the measured DFT transient spectra is shown in Fig. 3 which illustrates typical real-time spectral evolution over hundreds of roundtrips with several obvious features.

At the beginning of such pulsating period, ignited by modulation instability (MI), signal pulse grows slightly in several roundtrips. There exist multiple spectral components indicated with red arrows in Fig. 3 (b), which is reminiscent of primitive DFT observation in build-up of mode locking [25] and dissipative soliton formation [26]. Moreover, note that MI could be efficiently driven in microfiber of anomalous dispersion [7].

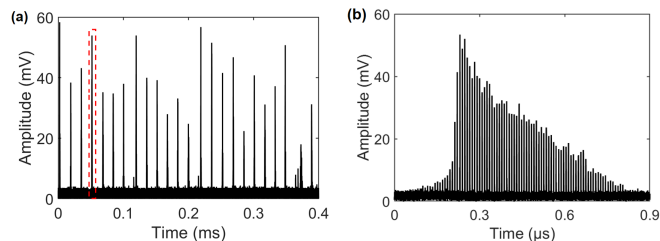


FIG. 2. Temporal measurement results. (a) The temporal train of QS-NLP in ms scale. (b) The zoom-in QS-NLPs intensity dynamics in μ s scale red boxed in (a), where the pulse power undergoes exponential growth and then decay to negligible level due to strong dissipation.

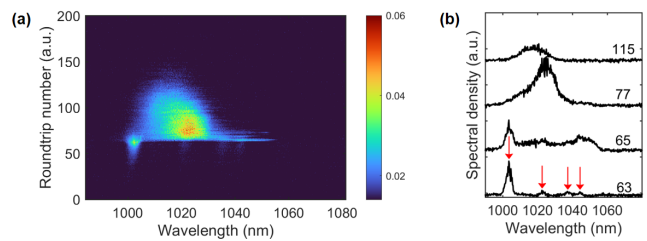


FIG. 3. Typical DFT experiment result of single Q-switched envelope. (a) Single-shot spectra and (b) its sliced spectra at particular roundtrips. The red arrows indicate the initial spectral components related to MI.

Following the above preliminary amplification process, the spectral sideband at ~ 1030 nm with maximum gain is exponentially amplified in several roundtrips at the expense of pump. Meanwhile, stemming from the combined high nonlinearity and anomalous dispersion of microfiber [7], the spectra broaden abruptly.

As the pulse energy grows in a short time and meanwhile saturates the gain, the transient broadband spectra in particular of those components beyond gain bandwidth do not survive in the following roundtrips. Furthermore, the spectrum continue narrowing down as long as loss surpass gain.

In addition to the above DFT measurement, basic characterization of QS-NLP was exhibited in [7]. But overall, experimental measurement only provides presentational spectral-temporal intensity dynamics, the underlying slow gain dynamics uncovered in earlier solid-state laser experiment [27] probably gives rise to the observed pattern formations and we will demonstrate it theoretically.

III. SIMULATION MODELING

In this section we give the pulse propagation model in fiber laser incorporating slow gain dynamics. Detailed fiber parameters in particular of microfibers (e.g. when diameter is ~ 1.2 μ m, $\gamma = 182.2$ $W^{-1} km^{-1}$ and $\beta_2 = -156.6$ ps^2/km) used here refer to [28, 29] and have been shown in previous experiment [7].

A. Gain dynamics modeling

The gain dynamics related rate equations in Yb-doped fiber is modeled like Er-doped amplifiers with two-level character when ignoring the effect of amplified sponta-

neous emission (ASE) [16, 30, 31]:

$$\begin{cases} N_t = N_0(z, t) + N_1(z, t) \\ \frac{\partial N_1(z, t)}{\partial t} = \frac{I_s}{h\nu_s} (N_0(z, t)\sigma_s^a - N_1(z, t)\sigma_s^e) + \\ \frac{I_p}{h\nu_p} (N_0(z, t)\sigma_p^a - N_1(z, t)\sigma_p^e) - \frac{N_2(z, t)}{\tau_2} \end{cases} \quad (1)$$

where N_t , N_0 , N_1 are the total population concentration, lower level population and upper level population, respectively. $I_s(I_p)$, $\nu_s(\nu_p)$, $\sigma_s^a(\sigma_p^a)$, $\sigma_s^e(\sigma_p^e)$ are the signal(pump) intensity, frequency, absorption and emission cross-section, h is the Planck constant, τ_2 is the upper laser level lifetime.

The gain coefficient $g(z, P_{\text{avg}}, \lambda) = g_m(z, P_{\text{avg}})g(\lambda)$ when pulse propagates along gain fiber is defined as [29, 32]:

$$\begin{cases} g_m(z, P_{\text{avg}}) = \frac{\partial (\ln P_s(z))}{\partial z} \\ = \Gamma_s (N_1(z)\sigma_s^e - N_0(z)\sigma_s^a) \\ g(\lambda) = e^{-\left(\frac{\lambda-\lambda_0}{\Delta\lambda}\right)^2} \end{cases} \quad (2)$$

in which $g(\lambda)$ is related to Gaussian spectral response near at $\lambda_0 \sim 1030$ nm with gain bandwidth $\Delta\lambda$, Γ_s is the signal overlap integral [15, 16] and P_{avg} corresponds to the average power along the gain fiber.

When assuming a constant, uniform pump along the gain fiber (although impractical, as shown in [4], it does not obscure the physical processes to explain), we can derive the fast gain dynamics equation similar to [4] after combining Eq. (1) and Eq. (2):

$$\frac{\partial g_m}{\partial t} = -\left(\frac{1}{\tau_e} + \frac{P_s}{P_{s,\text{sat}} \cdot \tau_e}\right) g_m + \Lambda \quad (3)$$

where $\tau_e = \tau_2 / (1 + P_p/P_T)$ is the effective upper laser level lifetime with pump transparency power $P_T = h\nu_p A_{\text{eff},p} / [(\sigma_p^a + \sigma_p^e) \tau_2]$ [16] and pump power $P_p = I_p A_{\text{eff},p} = h\nu_p \phi_p A_{\text{eff},p}$; $P_{s,\text{sat}} = h\nu_s A_{\text{eff},s} / [(\sigma_s^a + \sigma_s^e) \tau_e]$ is the signal saturation power [4]; the constant $\Lambda = -\Gamma_s N_t \sigma_s^a / \tau_2 - \Gamma_s \phi_p N_t (\sigma_s^a \sigma_p^e - \sigma_s^e \sigma_p^a)$ accounts for the influence of pump in excess, $\Lambda \cdot \tau_e$ is equivalent to the well-known small-signal gain coefficient [29]; and P_s is the signal power.

It is worth noting that similar gain dynamics formula proposed in [29] with realistic upper level lifetime τ_2 is replaced by τ_e in Eq. (3) and there is usually two orders of magnitude difference between them. This pump induced transient response within effective lifetime τ_e can be traced back primitive research of EDFA in WDM systems [33, 34].

In the mean-field model, the fast gain dynamics that mainly affects the inner structure of pulse wavepacket [17] is neglected and we only consider the roundtrip-to-roundtrip slow gain dynamics in the unit of round-trip time T_R . Based on multi-scale perturbation approach

[35], we obtain the similar slow gain dynamics equation proposed in [21, 22] expressed as:

$$T_R \frac{\partial g_m}{\partial T} = -\left(\frac{T_R}{\tau_e} + \frac{\int_0^{T_R} |A(T, t)|^2 dt}{P_{s,\text{sat}} \cdot \tau_e}\right) g_m + T_R \cdot \Lambda \quad (4)$$

in which $T = n \cdot T_R$ is the slow-time variable and n is an integer.

Furthermore, in the slow gain form Eq. (4) could be written as:

$$\frac{\partial g_m}{\partial T} = -\left(\frac{1}{\tau_e} + \frac{\langle P_s \rangle}{P_{s,\text{sat}} \cdot \tau_e}\right) g_m + \Lambda \quad (5)$$

where $\langle P_s \rangle = \frac{1}{T_R} \int_0^{T_R} |A(T, t)|^2 dt$ is intracavity signal average power. Eq. (5) is the ultimate equation describing the roundtrip-to-roundtrip slow gain dynamics for simulation.

Besides, the utilized parameters of YDF [16, 30, 31] for modeling are listed in Table I.

TABLE I. Simulation parameters of YDF

Parameter	Value
length, l	0.2 m
dopant radius, b	2.0* μm
pump power, P_p	0.6 W
upper level lifetime, τ_2	770 μs
Yb ³⁺ concentration, N_t	1.2×10^{26} * m^{-3}
mode field radius, w_s/w_p	2.2/2 μm
overlap integral, Γ_s/Γ_p	0.56/0.63
absorption cross section, σ_p^a/σ_s^a	$2.5/0.05 \times 10^{-24}$ m^2
emission cross section, σ_p^e/σ_s^e	$2.5/0.6 \times 10^{-24}$ m^2

* Undisclosed values.

B. Pulse propagation modeling

The schematic configuration of the fiber laser is shown in Fig.1, which consist of a section of 0.2 m microfiber with diameter of 1.2 μm , a piece of 0.2 m Yb-doped fiber (LIEKKI® Yb1200-4/125) and remaining of 1.3-m-long SMF (HI1060).

We model the fiber laser with generalized nonlinear Schrodinger equation [32], i.e.,

$$\begin{aligned} \frac{\partial A}{\partial z} - \sum_{k=2}^4 \frac{i^{k+1}}{k!} \beta_k \frac{\partial^k A}{\partial t^k} - \frac{g(z, P_{\text{avg}}, \omega)}{2} A \\ = i\gamma \left(1 + \frac{i}{\omega_0} \frac{\partial}{\partial t}\right) \left[A(z, t) \int_{-\infty}^{\infty} R(t') |A(z, t-t')|^2 dt'\right] \end{aligned} \quad (6)$$

where terms on the right hand side responsible for stimulated Raman scattering (SRS) and SPM are included; $g(z, P_{\text{avg}}, \omega)$ is the gain coefficient (otherwise set as zero for passive fiber) described by Eq. (2) and Eq. (5).

For convenience, in simulation we only focus on the slow gain dynamics at signal wavelength (~ 1030 nm) and

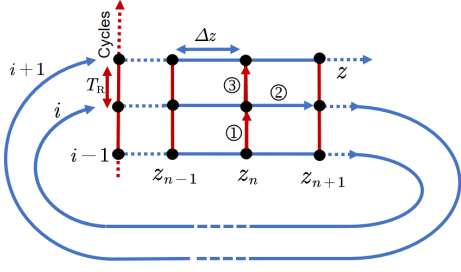


FIG. 4. Schematic of the numerical calculation procedure of pulse propagation in YDF. Red lines correspond to gain evolution over cycles in the unit of T_R while the blue lines associated with pulse propagation in each cycle. Circled numbers indicate the calculation steps at each node.

ignore other spectral components even though whose dynamic evolution exist as shown in Fig. 3.

Numerical treatment of single pulse propagation in YDF is similar to [4] and shown in Fig. 4. Before considering the pulse profile $A(T_i, z_n)$ at the point z_n in i -th cycle, the gain $g(T_i, z_n)$ should be evaluated by integrating Eq. (5) over T_R in advance, as expressed in Eq. (7). Afterwards such gain coefficient allows determining the pulse profile at z_{n+1} with Eq. (6). Besides, the pulse profile $A(T_i, z_n)$ determines the local averaged power $\langle P_s(z_n) \rangle$, which in turn influence the $g(T_{i+1}, z_n)$ in next cycle. We can repeat the procedure to simulate the buildup dynamics of QS-NLP in such fiber laser.

$$\begin{cases} g(T_i, z_n) = g(T_{i-1}, z_n) + \int_{T_{i-1}}^{T_i} \frac{\partial g(T_{i-1}, z_n)}{\partial T} dT \\ A(T_i, z_{n+1}) = A(T_i, z_n) + \int_{z_n}^{z_{n+1}} \frac{\partial A(T_i, z_n, g(T_i, z_n))}{\partial z} dz \end{cases} \quad (7)$$

Prior to simulation, we set the initial gain to the small-signal value at all position along the YDF. An sech-shape small signal (peak power of $1 \mu\text{W}$) plusing Gaussian background noise is fed into fiber laser initially to accelerate the convergence of calculation.

Finally, typical parameters value of intracavity elements are listed as follow [7, 36]:

(i) YDF: $\gamma = 11.5 \text{ W}^{-1} \text{ km}^{-1}$; $\beta_2 = 26.2 \text{ ps}^2/\text{km}$, $\beta_3 = -0.0134 \text{ ps}^3/\text{km}$.

(ii) SMF: $\gamma = 5.9 \text{ W}^{-1} \text{ km}^{-1}$; $\beta_2 = 24.8 \text{ ps}^2/\text{km}$, $\beta_3 = -0.0233 \text{ ps}^3/\text{km}$.

(iii) MF: $\gamma = 182.2 \text{ W}^{-1} \text{ km}^{-1}$; $\beta_2 = -156.6 \text{ ps}^2/\text{km}$, $\beta_3 = 0.152 \text{ ps}^3/\text{km}$, $\beta_4 = 1.55 \times 10^{-4} \text{ ps}^4/\text{km}$.

(iv) SA: $T = 1 - l_0 / [1 + P_s(t) / P_{\text{sat}}]$ with $l_0 = 0.84$ and $P_{\text{sat}} = 90 \text{ W}$.

IV. RESULTS AND DISCUSSION

Experimentally, as mentioned before that the QS-NLP could easily self-start at certain intracavity polarization, i.e. specific SA transmission function T . It is well-known that SA always provides positive feedback in the self-starting mode-locking process where the main pulses

strat up from initial noise fluctuation formed by mode-beating [37], while NLP self-starting process usually involves subsequently further increment in the pulse power that instead lead to negative feedback of SA [9]. In the condition of high linear intracavity loss, only at these locations where previous main pulses disturbed can the dispersive wave, collapsed soliton components or background noise generate, undergo amplification and further circulate as bunch temporally [38, 39]. As a result, such low coherence components bunched NLP presents typical double-scale (fs-ps) temporal autocorrelation profile [7] and apparent spectral roundtrip-to-roundtrip fluctuations[40, 41].

We emphasize that the laser always radiates quasi-periodically (intuitive display refers to Fig. 3 (a) in [7]). In simulation, for simplicity we only focus on laser dynamics within single Q-switched envelope. Fig. 5 shows the typical numerical results in hundreds of roundtrips. We could observe that the simulated spectral profile fits well to the experimental one in Fig. 5 (a).

According to Fig. 5 (b), we can directly observe the underlying dynamic evolution of both gain and loss(counts the influence of SA and OC) within Q-switched envelope. Considering together with Fig. 5 (d), we can find that at the amplification stage the saturatable gain and loss decrease synchronously along with rapid growth of pulse energy. After that loss prevails over gain, hinges with pulse power and thus leads to a slowly decaying trail of Q-switched envelope.

The spectral dynamic evolution is shown in Fig. 5 (c). We can find the spectrum could broaden abruptly and then narrows down, which is qualitatively similar to the

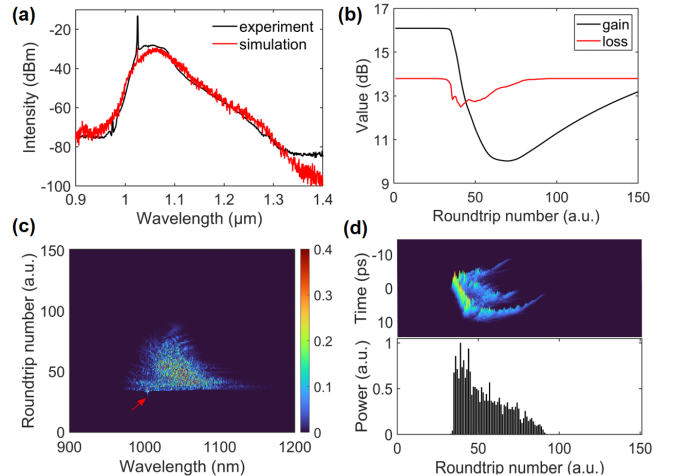


FIG. 5. Simulation of single QS-NLP dynamics over 150 roundtrips. (a) Averaged simulation spectrum and experimental result. (b) Gain/loss level evolution over roundtrips, there come into being QS-NLPs when gain surpasses loss [27]. (c) Simulated spatio-temporal spectral dynamics in linear scale, the red arrow indicates the initial small signal. (d) Upper panel: temporal intensity dynamics over roundtrips; lower panel: pulse peak value evolution over roundtrips.

experimental observation in Fig. 3 (c) although ignoring initial multiple spectral components.

Lastly, as we only consider the artificial SA in a quite simple generalized formula, the simulation is unable to fully reproduce the experimental observation and insufficient for accurate exploration of other unconcerned experimental valuable parameters such as Q-switched envelope period and Q-switching stability limits [24, 42]. Further detailed experimental parameters access by either intracavity precise polarization management [43] or changing the laser structure [32] will be helpful for deeper exploring of the relevant underlying mechanism.

V. CONCLUSION

In summary, based on a simple gain dynamics model we demonstrate that, in our highly dissipative fiber laser, the Q-switched characteristic of NLP is attributed to the combined impact of gain dynamics (saturable gain depletes rapidly whereas recovers slowly) and SA effect.

The proposed convenient numerical model here we believe that not only provides essential insight into the operational dynamics of experimentally realized architectures like RWs [7, 44, 45] and other nonlinear phenomena involving Q-switching instabilities [46, 47], but also allows for simple and fast exploration of various parameter regimes so as to discover new laser designs with improved performance, e.g. high peak power broadband light source [48].

ACKNOWLEDGMENTS

We thank Wenbin He for inspired discussions. This work was supported by the National Key Research and Development Program of China (Grants No. 2020YFC2200403), National Natural Science Foundation of China (Grants No. 62175122 and Grants No. 61905213).

Appendix A: Gain dynamics over consecutive Q-switched envelopes

In order to provide more intuitive insight into the slow gain dynamics over much longer roundtrips than shown in Fig. 5. Here we also calculate the envelope-to-envelope gain dynamics shown in Fig. 6. We can see the pronounced dynamic evolution of slow gain as well as fast saturation absorption loss.

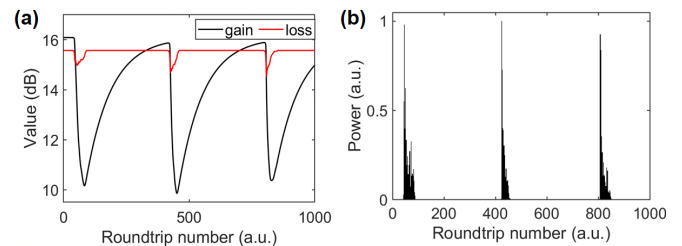


FIG. 6. (a) Gain/loss evolution over sequences of Q-switched envelopes. (b) Temporal QS-NLP intensity dynamics.

-
- [1] J. M. Dudley, F. Dias, M. Erkintalo, *et al.*, Instabilities, breathers and rogue waves in optics, *Nat. Photon.* **8**, 755 (2014).
 - [2] P. Grelu and N. Akhmediev, Dissipative solitons for mode-locked lasers, *Nat. Photon.* **6**, 84 (2012).
 - [3] M. Horowitz, Y. Barad, and Y. Silberberg, Noiselike pulses with a broadband spectrum generated from an erbium-doped fiber laser, *Opt. Lett.* **22**, 799 (1997).
 - [4] O. Pottiez, J. Lauterio-Cruz, Y. Bracamontes-Rodríguez, *et al.*, Gain-driven spectral-temporal noise-like pulse dynamics in a passively mode-locked fiber laser, *Opt. Express* **27**, 34742 (2019).
 - [5] X. Wei, Y. Xu, and K. K. Y. Wong, 1000-1400-nm partially mode-locked pulse from a simple all-fiber cavity, *Opt. Lett.* **40**, 3005 (2015).
 - [6] C. Lecaplain, P. Grelu, J. M. Soto-Crespo, *et al.*, Dissipative rogue wave generation in multiple-pulsing mode-locked fiber laser, *J. Opt.* **15**, 064005 (2013).
 - [7] J. Zhou, Y. Li, Y. Ma, *et al.*, Broadband noise-like pulse generation at 1 μ m via dispersion and nonlinearity management, *Opt. Lett.* **46**, 1570 (2021).
 - [8] U. Keller, Recent developments in compact ultrafast lasers, *Nature* **424**, 831 (2003).
 - [9] Y. Jeong, L. A. Vazquez-Zuniga, S. Lee, *et al.*, On the formation of noise-like pulses in fiber ring cavity configurations, *Opt. Fiber Technol.* **20**, 575 (2014).
 - [10] K. Goda and B. Jalali, Dispersive fourier transformation for fast continuous single-shot measurements, *Nat. Photon.* **7**, 102 (2013).
 - [11] S. Sun, Z. Lin, W. Li, *et al.*, Time-stretch probing of ultra-fast soliton dynamics related to Q-switched instabilities in mode-locked fiber laser, *Opt. Express* **26**, 20888 (2018).
 - [12] D. V. Churkin, S. Sugavanam, N. Tarasov, *et al.*, Stochasticity, periodicity and localized light structures in partially mode-locked fibre lasers, *Nat. Commun.* **6**, 7004 (2015).
 - [13] O. Pottiez, R. G.-C. no, B. Ibarra-Escamilla, *et al.*, Adjustable noiselike pulses from a figure-eight fiber laser, *Appl. Opt.* **50**, E24 (2011).
 - [14] Y. Kwon, L. A. Vazquez-Zuniga, S. Lee, *et al.*, Numerical study on multi-pulse dynamics and shot-to-shot coherence property in quasi-mode-locked regimes of a highly-pumped anomalous dispersion fiber ring cavity, *Opt. Express* **25**, 4456 (2017).
 - [15] C. R. Giles and E. Desurvire, Modeling erbium-doped fiber amplifiers, *J. Lightwave Technol.* **9**, 271 (1991).

- [16] C. Barnard, P. Myslinski, J. Chrostowski, *et al.*, Analytical model for rare-earth-doped fiber amplifiers and lasers, *IEEE J. Quantum Electron.* **30**, 1817 (1994).
- [17] A. Zaviyalov, P. Grelu, and F. Lederer, Impact of slow gain dynamics on soliton molecules in mode-locked fiber lasers, *Opt. Lett.* **37**, 175 (2012).
- [18] R. Weill, A. Bekker, V. Smulakovsky, *et al.*, Noise-mediated Casimir-like pulse interaction mechanism in lasers, *Optica* **3**, 189 (2016).
- [19] J. N. Kutz, B. C. Collings, K. Bergman, *et al.*, Stabilized pulse spacing in soliton lasers due to gain depletion and recovery, *IEEE J. Quantum Electron.* **34**, 1749 (1998).
- [20] S. V. Smirnov, S. Sugavanam, O. A. Gorbunov, *et al.*, Generation of spatio-temporal extreme events in noise-like pulses NPE mode-locked fibre laser, *Opt. Express* **25**, 23122 (2017).
- [21] N. Englebort, C. M. Arabí, P. Parra-Rivas, *et al.*, Temporal solitons in a coherently driven active resonator, *Nat. Photon.* **15**, 536 (2021).
- [22] N. Englebort, F. D. Lucia, P. Parra-Rivas, *et al.*, Parametrically driven Kerr cavity solitons (2021), [arXiv:2101.07784](https://arxiv.org/abs/2101.07784).
- [23] T. J. Kippenberg, J. Kalkman, A. Polman, *et al.*, Demonstration of an erbium-doped microdisk laser on a silicon chip, *Phys. Rev. A* **74**, 051802 (2006).
- [24] C. Hönniger, R. Paschotta, F. Morier-Genoud, *et al.*, Q-switching stability limits of continuous-wave passive mode locking, *J. Opt. Soc. Am. B* **16**, 46 (1999).
- [25] G. Herink, B. Jalali, C. Ropers, *et al.*, Resolving the build-up of femtosecond mode-locking with single-shot spectroscopy at 90 MHz frame rate, *Nat. Photon.* **10**, 321 (2016).
- [26] J. Peng, M. Sorokina, S. Sugavanam, *et al.*, Real-time observation of dissipative soliton formation in nonlinear polarization rotation mode-locked fibre lasers, *Commun. Phys.* **1**, 20 (2018).
- [27] F. X. Kaertner, L. R. Brovelli, D. Kopf, *et al.*, Control of solid state laser dynamics by semiconductor devices, *Opt. Eng.* **34**, 2024 (1995).
- [28] L. Tong, J. Lou, and E. Mazur, Single-mode guiding properties of subwavelength-diameter silica and silicon wire waveguides, *Opt. Express* **12**, 1025 (2004).
- [29] G. P. Agrawal, *Applications of nonlinear fiber optics* (Academic Press, 2007).
- [30] R. Paschotta, J. Nilsson, A. C. Tropper, *et al.*, Ytterbium-doped fiber amplifiers, *IEEE J. Quantum Electron.* **33**, 1049 (1997).
- [31] H. M. Pask, R. J. Carman, D. C. Hanna, *et al.*, Ytterbium-doped silica fiber lasers: versatile sources for the 1-1.2 μm region, *IEEE J. Quantum Electron.* **1**, 2 (1995).
- [32] A. F. J. Runge, C. Aguergaray, R. Provo, *et al.*, All-normal dispersion fiber lasers mode-locked with a nonlinear amplifying loop mirror, *Opt. Fiber Technol.* **20**, 657 (2014).
- [33] Y. Sun, J. L. Zyskind, A. K. Srivastava, *et al.*, Analytical formula for the transient response of erbium-doped fiber amplifiers, *Appl. Opt.* **38**, 1682 (1999).
- [34] E. Desurvire, Analysis of transient gain saturation and recovery in erbium-doped fiber amplifiers, *IEEE Photonics Technol. Lett.* **1**, 196 (1989).
- [35] A. Haboucha, H. Leblond, M. Salhi, *et al.*, Analysis of soliton pattern formation in passively mode-locked fiber lasers, *Phys. Rev. A* **78**, 043806 (2008).
- [36] Çağrı Şenel, R. Hamid, C. Erdoğan, *et al.*, Tailored design of mode-locking dynamics for low-noise frequency-comb generation, *Phys. Rev. Appl.* **10**, 024027 (2018).
- [37] L. E. Nelson, D. J. Jones, K. Tamura, *et al.*, Ultrashort-pulse fiber ring lasers, *Appl. Phys. B* **65**, 277 (1997).
- [38] D. Y. Tang, L. M. Zhao, and B. Zhao, Soliton collapse and bunched noise-like pulse generation in a passively mode-locked fiber ring laser, *Opt. Express* **13**, 2289 (2005).
- [39] L. M. Zhao, D. Y. Tang, J. Wu, *et al.*, Noise-like pulse in a gain-guided soliton fiber laser, *Opt. Express* **15**, 2145 (2007).
- [40] C. Lecaplain and P. Grelu, Rogue waves among noise-like pulse laser emission: An experimental investigation, *Phys. Rev. A* **90**, 013805 (2014).
- [41] A. F. J. Runge, C. Aguergaray, N. G. R. Broderick, *et al.*, Coherence and shot-to-shot spectral fluctuations in noise-like ultrafast fiber lasers, *Opt. Lett.* **38**, 4327 (2013).
- [42] H. Cheng, W. Lin, T. Qiao, *et al.*, Theoretical and experimental analysis of instability of continuous wave mode locking: Towards high fundamental repetition rate in Tm^{3+} -doped fiber lasers, *Opt. Express* **24**, 29882 (2016).
- [43] G. Pu, L. Yi, L. Zhang, *et al.*, Intelligent programmable mode-locked fiber laser with a human-like algorithm, *Optica* **6**, 362 (2019).
- [44] A. Zaviyalov, O. Egorov, R. Iliev, *et al.*, Rogue waves in mode-locked fiber lasers, *Phys. Rev. A* **85**, 013828 (2012).
- [45] J. M. Soto-Crespo, P. Grelu, and N. Akhmediev, Dissipative rogue waves: Extreme pulses generated by passively mode-locked lasers, *Phys. Rev. E* **84**, 016604 (2011).
- [46] Z. Wang, Z. Wang, Y. Liu, *et al.*, The simultaneous generation of soliton bunches and Q-switched-like pulses in a partially mode-locked fiber laser with a graphene saturable absorber, *Laser Phys. Lett.* **15**, 055101 (2018).
- [47] T. Qiao, W. Chen, W. Lin, *et al.*, Generation of Q-switched mode locking controlled rectangular noise-like soliton bunching in a Tm-doped fiber laser, *Opt. Express* **24**, 18755 (2016).
- [48] S. V. Chernikov, Y. Zhu, J. R. Taylor, *et al.*, Supercontinuum self-Q-switched ytterbium fiber laser, *Opt. Lett.* **22**, 298 (1997).